Optica Applicata, Vol. LV, No. 3, 2025
DOI: 10.37190/oa/205600

Analytical study of the self-reconstruction of a Hermite non-uniformly correlated beams by an obstacle

XIANYANG YANG[1], WENYU FU[2,*]

[1] School of Intelligent Manufacturing and Energy Engineering, Jiang-Xi University of Engineering, Xinyu, 33800, Jiangxi, China

[2] School of Electronic Information Engineering, Jiang-Xi University of Engineering Xinyu, 33800, Jiangxi, China

[*]Corresponding author: qytcfwy@163.com

In this study, we derived a theoretical formula to analyze the self-constructing properties of Hermite non-uniformly correlated (HNUC) beams when encountering an obstacle, focusing on intensity and coherence. Our results reveal that, despite an obstacle, the beam's intensity distribution continues to display a significant self-focusing phenomenon. Within the focal length range, the lateral intensity distribution remains consistent with unobstructed propagation, regardless of the obstacle's size. However, outside the self-focusing range, increasing the obstacle size leads to a decrease in the self-reconstructive capability of the intensity distribution, necessitating a longer propagation distance for recovery. Additionally, the presence of obstacles considerably impacts the coherence properties of the beams. When the obstacle is small, the degree of coherence (DOC) experiences a significant reconstructing effect. Our results have potential applications in optical tweezers, microscopy, and optical communication.

Keywords: self-reconstruction, Hermite non-uniformly correlated beams, similarity degree, self-focusing.

1. Introduction

The spatial coherence of a laser beam, as its fundamental characteristic, directly affects the propagation behaviour of the beam. When spatial coherence decreases, the partially coherent beam formed often exhibits unique advantages over fully coherent beams [1-3]. Specifically, beams with non-uniform spatial correlation functions (*i.e.*, non-uniform correlation structured beams) exhibit novel characteristics such as self -focusing, self-splitting, and self-shifting during propagation due to their non-traditional coherence distribution [4-6]. Since the Gori team established the theoretical basis for designing spatial correlation functions [7, 8], the researchers have successfully developed new light sources, including non-uniform Laguerre Gaussian correla-

tion beams, pseudo-Bessel correlation beams, and radially polarized Hermitian beams by constructing various non-Gaussian correlation functions [9-14], greatly expanding the research dimension of non-uniform correlation beams.

The self-reconstructive property of a beam refers to its ability to reconstruct the initial propagation characteristics after environmental interference, which has been validated in various beam systems. Early research first observed self-reconstructing phenomena in zero-order Bessel beams [15], followed by systematic studies in non-diffractive beams such as Bessel Gaussian beams [16]. As our understanding deepens, research has found that self-reconstructing properties are not exclusive to nondiffractive beams: vector Laguerre Gaussian beams [17], tightly focused Bessel Gaussian beams [18], and partially coherent beams all exhibit this property [19,20]. Notably, the radial polarized Schell model beam exhibits excellent self-reconstructing ability regarding intensity distribution and polarization state when encountering obstacle scattering [20]. Many studies have further revealed the influence of different parameters on the self-reconstructing process, including the circular dislocation reconstruction phenomenon of partially coherent LG beam coherence discovered by LIU *et al.* [21], the regulatory effect of vortex phase distortion factor on self-healing confirmed by Peng's team [22], and the self-reconstructing in intensity distribution, polarization, and coherence properties after disturbed propagation studied by ZHOU *et al.* [23]. However, so far, research has only been limited to uniformly coherent structured beams, and there have been no reports on whether there is a self-reconstructive phenomenon in the propagation of non-uniform correlated structured beams.

Based on the above research background, we select a Hermitian non-uniform correlated (HNUC) beam as the model and, through systematic numerical simulation, reveal the evolution law of the propagation characteristics after obstacle scattering. We also quantitatively analyze the regulation mechanism of light source parameters and obstacle size on the self-reconstructing behaviour of the beam.

2. Theoretical evidence

The spatial coherence properties of a scalar HNUC beam are characterized by the cross-spectral density (CSD) in the space-frequency domain and the mutual coherence function in the space-time domain. The CSD is the quantity of choice for studying quasi-monochromatic fields, and it is defined as a two-point correlation function [24].

$$W(r_1, r_2) = \langle E^*(r_1) E(r_2) \rangle \tag{1}$$

where $r_1 = (x_1, y_1)$ and $r_2 = (x_2, y_2)$ are two arbitrary position vectors transverse to the direction of propagation, $E(r)$ represents the field fluctuating in a direction perpendicular to the z-axis, the asterisk denotes the complex conjugate, and the angular brackets denote a monochromatic ensemble average.

The CSD of scalar HNUC can be expressed in the following general form

$$W(r_1, r_2) = \int p(v) H^*(r_1, v) H(r_2, v) \mathrm{d}v \tag{2}$$

where $p(v)$ is a non-negative weight function, $H(r_1, v)$ and $H(r_2, v)$ are two arbitrary kernels. We take $H(r, v)$ to be a kernel of the form

$$H(\rho, v) = \exp\left(-\frac{r^2}{2\sigma^2}\right)\exp(-ikvr^2) \tag{3}$$

$$p(v) = \frac{1}{\pi a^2}\left(\frac{2v}{a^2}\right)^{2n}\exp\left(-\frac{v^2}{a^2}\right) \tag{4}$$

where the beam widths are denoted by σ. Substituting Eqs. (3) and (4) into Eq. (2), and we derive the CSD of the beam as the following expression

$$W(r_1, r_2) = A_0\exp\left(-\frac{r_1^2 + r_2^2}{2\sigma^2}\right)\exp\left[-\frac{(r_1^2 - r_2^2)^2}{r_c^4}\right]H_{2m}\left(\frac{r_1^2 - r_2^2}{r_c^2}\right) \tag{5}$$

where $r_c = (2/ka)^{1/2}$ is the correlation width, $A_0 = 1/H_{2n}(0)$ and $H_{2n}(\cdot)$ denotes the Hermite polynomials order $2n$.

The propagation of the HNUC beams obstructed by nontransparent obstacles is shown in Fig. 1, and the CSD matrix of the beams can be obtained using the following expression.

$$W(\rho_1, \rho_2, v, z) = \left(\frac{1}{\lambda B}\right)^2\iiiint T^*(r_1)T(r_2)W(r_1, r_2) \times \exp\left\{-\frac{ik}{2B}\left[(r_1^2 - r_2^2) - 2(r_1\rho_1 - r_2\rho_2) + D(\rho_1 - \rho_2)^2\right]\right\}\mathrm{d}^2r_1\,\mathrm{d}^2r_2 \tag{6}$$

where $\rho_i = (x_i, y_i)$ is the transverse position vector in the receiver plane, A, B, C, and D are the optical system transfer matrix elements, and $T(r_i)$ is the transmittance func-

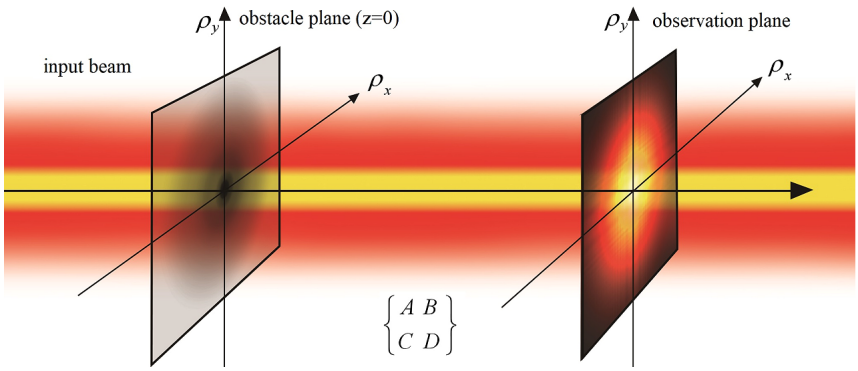

Fig. 1. Illustration of a HNUC beam self-reconstructing process.

tion of the opaque obstacle. We assume this obstacle is circular and has Gaussian absorption efficiency for convenience. Therefore, $T(r)$ could be written as [23]

$$T(r_i) = 1 - \exp\left[-\frac{(r_i - r_0)^2}{\omega_{\mathrm{d}}^2}\right] \tag{7}$$

in which $r_0 = (x_0, y_0)$ denotes the transverse position of the opaque obstacle in the source plane, and ω_{d} is the obstacle size. Substituting Eqs. (2) and (7) into Eq. (6), after tedious integration and simplification, we obtain the semi-analytical expressions of CSD matrix elements of the beam in the receiver plane.

$$W(\rho_1, \rho_2, z) = A_0\left(\frac{2\pi}{\lambda B}\right)^2 \exp\left[-\frac{ikD}{2B}(\rho_1 - \rho_2)^2 + \frac{ik}{B}(\rho_1 - \rho_2)r_0\right]$$

$$\times \iint p(v) P(\rho_1, \rho_2, z) \mathrm{d}^2 v \tag{8}$$

where

$$P(\rho_1, \rho_2, z) = \frac{2\pi\sigma^2}{\Delta_1} X_1 + \frac{2\pi w'^2}{\Delta_2} X_2 + \frac{2\pi w'^2}{\Delta_3} X_3 + \frac{2\pi \omega_{\mathrm{d}}'^2}{\Delta_4} X_4 \tag{9}$$

while

$$X_1 = \exp\left\{-\frac{\sigma^2 g^2}{4} - ir_0 g - \frac{k^2\sigma^2}{4B^2\Delta_1^2}\left[\left(1 + \sigma^2 f(v)\right)\rho_1 + \left(1 - \sigma^2 f(v)\right)\rho_2\right]^2\right\}$$

$$X_2 = \exp\left\{-\frac{w'^2 g^2}{4} - \frac{ir_0 w'^2 g^2}{\sigma^2} - \frac{r_0^2}{\sigma^2}\left(1 - \frac{w'^2}{\sigma^2}\right)\right.$$

$$\left. + \frac{w'^2}{\Delta_2^2}\left[\frac{ik}{2B}\left(1 - w'^2 F(v)\right)\rho_1 + \frac{ik}{2B}\left(1 + w'^2 F(v)\right)\rho_2 + r_0\left(f(v) + \frac{w'^2}{\sigma^2}F(v)\right)\right]^2\right\}$$

$$X_3 = \exp\left\{-\frac{w'^2 g^2}{4} - \frac{ir_0 w'^2 g^2}{\sigma^2} - \frac{r_0^2}{\sigma^2}\left(1 - \frac{w'^2}{\sigma^2}\right)\right.$$

$$\left. + \frac{w'^2}{\Delta_3^2}\left[\frac{ik}{2B}\left(1 + w'^2 F^*(v)\right)\rho_1 + \frac{ik}{2B}\left(1 - w'^2 F^*(v)\right)\rho_2 + r_0\left(f(v) - \frac{w'^2}{\sigma^2}F^*(v)\right)\right]^2\right\}$$

$$X_4 = \exp\left\{-\frac{\omega_d'^2\sigma^2 g^2}{4} - \frac{ir_0\omega_d'^2 g}{B} - \frac{r_0^2}{\sigma^2}(1-\omega_d'^2) + \frac{\omega_d'^2}{\Delta_4^2}\left[\frac{ik}{2B}\left(1+\omega_d'^2 f(v)\right)\rho_1 + \frac{ik}{2B}\left(1-\omega_d'^2 f(v)\right)\rho_2 + r_0\left(1-\frac{\omega_d'^2}{\sigma^2}\right)f(v)\right]^2\right\}$$

and

$$\frac{1}{w'^2} = \frac{1}{\sigma^2} + \frac{1}{\omega_d^2}, \qquad \frac{1}{\omega_d'^2} = \frac{2}{\omega_d^2} + \frac{1}{\sigma^2}$$

$$F(v) = \frac{1}{\omega_d^2} - f(v), \qquad f(v) = 2ik\left(v - \frac{A}{2B}\right), \qquad g = \frac{k}{B}(\rho_1 - \rho_2)$$

$$\Delta_1^2 = 1 - \sigma^4 f^2(v), \qquad \Delta_2^2 = 1 - w'^4 F^2(v),$$

$$\Delta_3^2 = 1 - w'^4 F^{*2}(v), \qquad \Delta_4^2 = 1 - \omega_d'^4 f^2(v)$$

Based on these formulas, we can conduct numerical studies on the propagation characteristics and self-reconstructing performance of the HNUC beams with obstacles.

3. Numerical example and analysis

In the following numerical examples, we explore the propagation characteristics of the HNUC beams under various light source parameters in free space when encountering opaque obstacles. The elements of the optical system transfer matrix are $A = 1$, $B = z$, and $D = 1$. Meanwhile, for the other parameters, we assume the following values: $\lambda = 632.8$ nm, $\sigma = 2$ mm, $r_c = 1$ mm, $n = 2$, $x_0 = 0$, $y_0 = 0$, unless otherwise indicated in figures. Firstly, we will investigate the self-reconstructive properties of the intensity distribution. The beam described by the CSD matrix has an average intensity in the observed plane from Eqs. (8) and (9) can be obtained as

$$S(\rho, z) = W(\rho, \rho, z) \tag{10}$$

Figure 2 illustrates the normalized intensity distribution of the HNUC beams at various distances in the presence of obstacles. It can be observed from Fig. 2 that when the beam encounters an obstacle, it does not diverge monotonically during propagation; instead, it maintains a notable self-focusing phenomenon. Additionally, within the focal length range, the lateral light intensity distribution remains consistent with unobstructed propagation, regardless of the size of the obstacle (as shown in Fig. 2(a4)–(a5), (b4)–(b5), (c4)–(c5), and (d4)–(d5)). This consistency is attributed to the diffraction

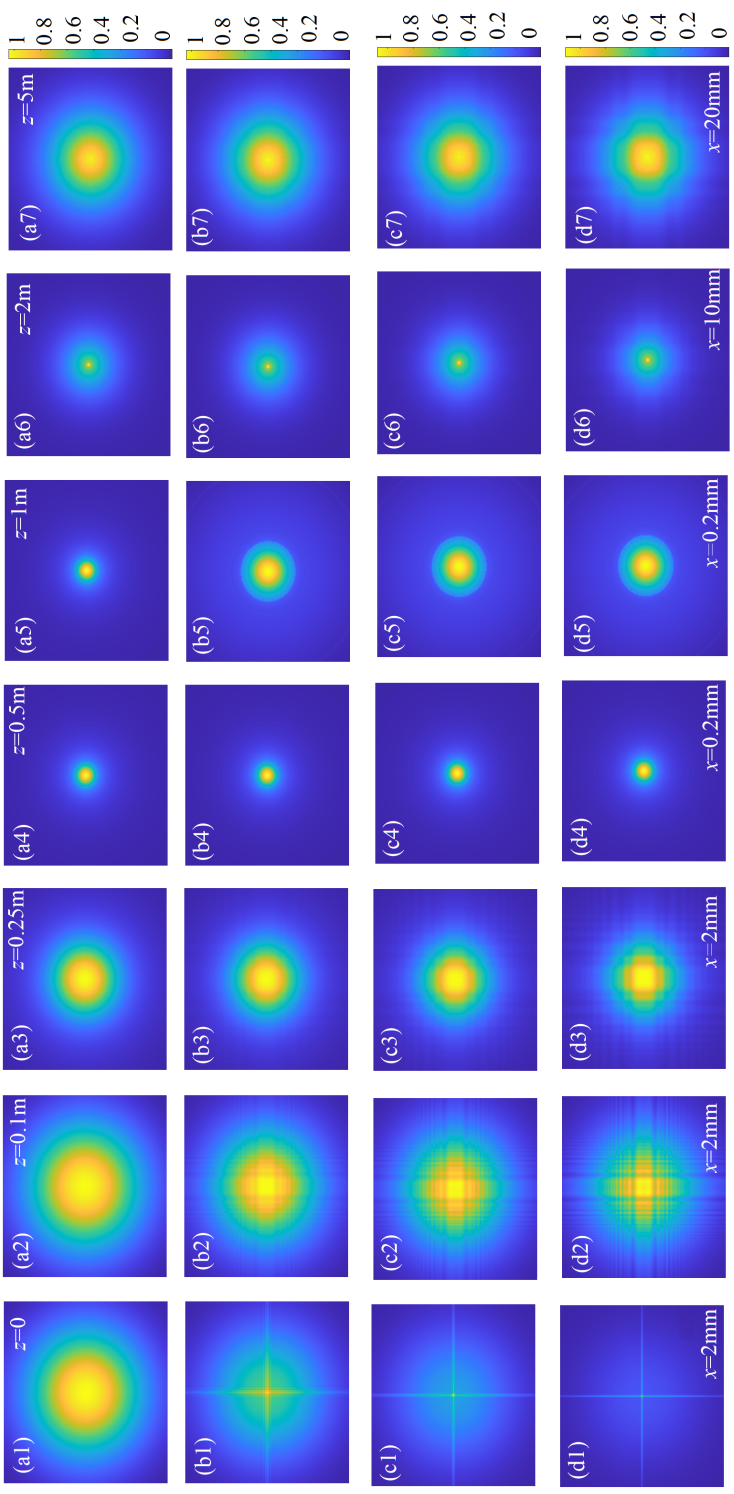

Fig. 2. Normalized intensity distributions of a HNUC beam with different obstacles at different propagating distances. As a comparison, the first row shows the results without the obstacle. (a) $\omega_d = 0$, (b) $\omega_d = 10$ μm, (c) $\omega_d = 25$ μm, and (d) $\omega_d = 50$ μm.

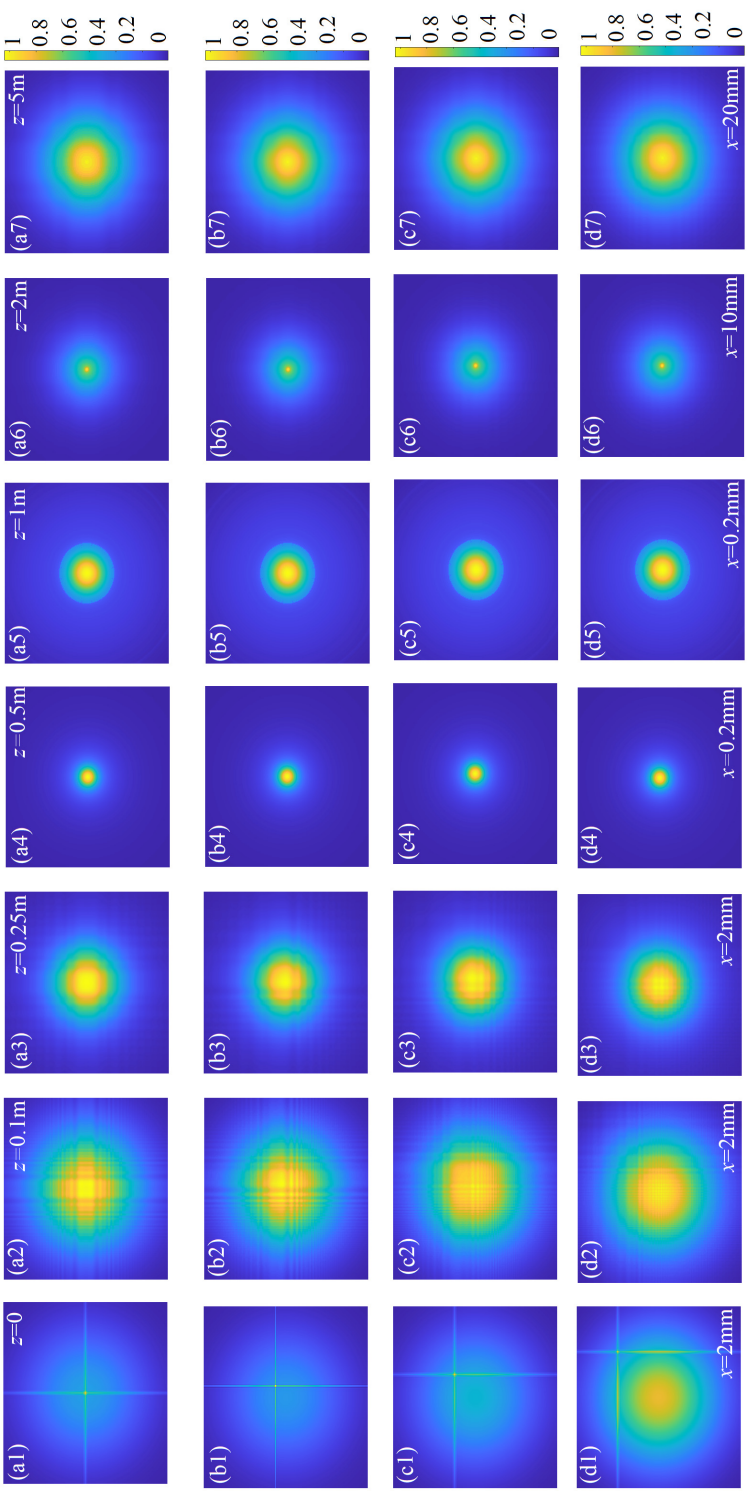

Fig. 3. Normalized intensity distributions of a HNUC beam with different transverse position coordinates of the obstacle at different propagating distances. As a comparison, the first row shows the results without the obstacle. (a) $x_0 = y_0 = 0$, $\omega_d = 10$ μm, (b) $x_0 = y_0 = 0.25$ mm, $\omega_d = 10$ μm, (c) $x_0 = y_0 = 0.5$ mm, $\omega_d = 10$ μm, and (c) $x_0 = y_0 = 1$ mm, $\omega_d = 10$ μm.

and scattering effects caused by the obstacles, which lead to beam divergence. However, the intrinsic properties of the HNUC beam promote convergence. The interplay between these factors results in complete self-restructuring of the HNUC beam within the focal length range. Beyond this range, obstacles distort the transverse intensity distribution of the HNUC beam. The larger the obstacle, the more pronounced the distortion of the intensity distribution becomes, requiring a greater propagation distance for the self-reconstructing process.

Figure 3 shows the influence of obstacles on the self-reconstructing ability of the HNUC beam intensity distribution at different propagation distances when obstacles are located at different positions of the transverse section. For easy comparison, the first row displays the result of obstacle position coordinates $x_0 = y_0 = 0$. From Fig. 3, it can be seen that as the obstacle position gradually deviates from the coordinate origin (as shown in Fig. 2(b1)–(b7), (c1)–(c7), and (d1)–(d7), the obstacle position coordinates increase from $x_0 = y_0 = 0.25$ mm to $x_0 = y_0 = 0.5$ mm, and finally to $x_0 = y_0 = 1$ mm), the scattering effect of the obstacle on the propagation of the beam gradually weakens, the distortion of the lateral intensity distribution also decreases, and compared with Fig. 3(a1)–(a7), the self-reconstructing ability of the HNUC beam significantly increases.

We use similarity degree to characterize the self-reconstruction ability in order to quantify the impact of obstacles and light source parameters on the beam. The detailed expression is as follows [19,20]

$$\gamma(z) = \frac{\iint S(\rho, z)\, S'(\rho, z)\mathrm{d}^2\rho}{\sqrt{\iint S(\rho, z)\,\mathrm{d}^2\rho}\ \sqrt{\iint S'(\rho, z)\mathrm{d}^2\rho}} \tag{11}$$

the $S(\rho, z)$ and $S'(\rho, z)$ represent the spectral density of the HNUC beam under conditions with and without an obstacle, respectively. According to the definition, the $\gamma(z)$ varies between 0 and 1. When $\gamma(z) = 1$, it indicates $S(\rho, z) = S'(\rho, z)$, meaning that obstacles do not affect the propagation of the beam. Therefore, we can assess the self -reconstructive ability of the beam by observing the changes in $\gamma(z)$.

Figure 4 shows how the similarity degree $\gamma(z)$ of the HNUC beam varies along the propagation distance z with different beam source parameters, particularly when the obstacle size is $\omega_\mathrm{d} = 50$ μm.

The analysis in Fig. 4 illustrates that the similarity degree of the HNUC beam increases rapidly, with significant fluctuations, until reaching a distance of 1 meter. Beyond this point, the increase slows and approaches a specific value closely related to the parameters of the beam source. This trend highlights the self-reconstructing nature of the HNUC beam. An obstacle in the source plane disrupts the HNUC beam, resulting in substantial differences between the obstructed beam and the original HNUC beam at shorter distances. However, as the beam propagates beyond 1 meter, the obstructed beam increasingly resembles the HNUC beam due to the self-reconstructing effect. Figure 4(a) shows how similarity degrees vary at different coherence lengths. When

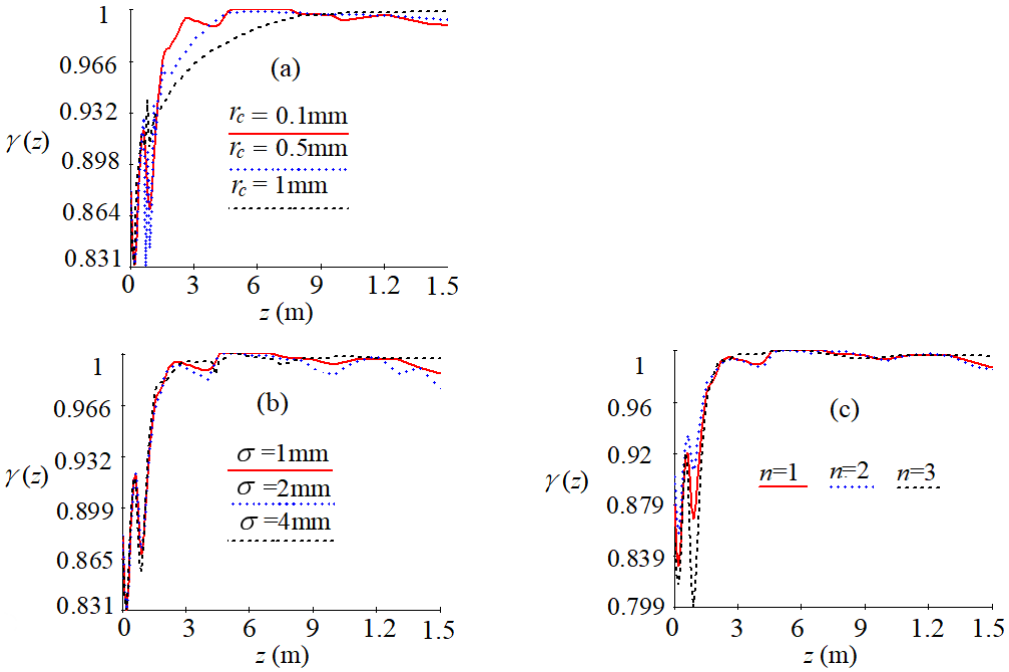

Fig. 4. The variation of similarity degree as a function of propagating distance with different beam source parameters when encountering an obstacle. (a) r_c = 0.1, 0.5, and 1 mm, ω_d = 50 μm, (b) σ = 1, 2, and 4 mm, ω_d = 50 μm, and (c) n = 1, 2, and 3, ω_d = 50 μm.

the propagation distance is less than 1 meter, beams with longer coherence lengths gradually achieve a similarity degree of 1 after experiencing notable fluctuations, especially when compared to those with shorter coherence lengths. Conversely, once the distance exceeds 1 meter, the similarity degree of beams with shorter coherence lengths tends to stabilize around a specific value after a decrease in fluctuations. These findings suggest that beams with longer coherence lengths are more likely to self-heal and retain the original beam's propagation characteristics. Figures 4(b) and (c) further illustrate the variation of the similarity degree with propagation distance for different beam widths and orders, respectively. The similarity degree of the light beam gradually stabilizes after experiencing fluctuations and an initial increase. In comparison, beams with greater beam widths and higher orders exhibit a higher similarity degree, indicating a stronger self-healing ability.

Next, we investigate the coherence self-reconstructive ability of the HNUC beam with an obstacle. According to the theory of coherence and polarization of light, the degree of coherence (DOC) for the HNUC beam at a pair of field points ρ_1 and ρ_2 can be written as

$$\mu(\rho_1, \rho_2, z) = \frac{\mathrm{Tr}\, W(\rho_1, \rho_2, z)}{\sqrt{\mathrm{Tr}\, W(\rho_1, \rho_2, z) \cdot \mathrm{Tr}\, W(\rho_1, \rho_2, z)}} \tag{12}$$

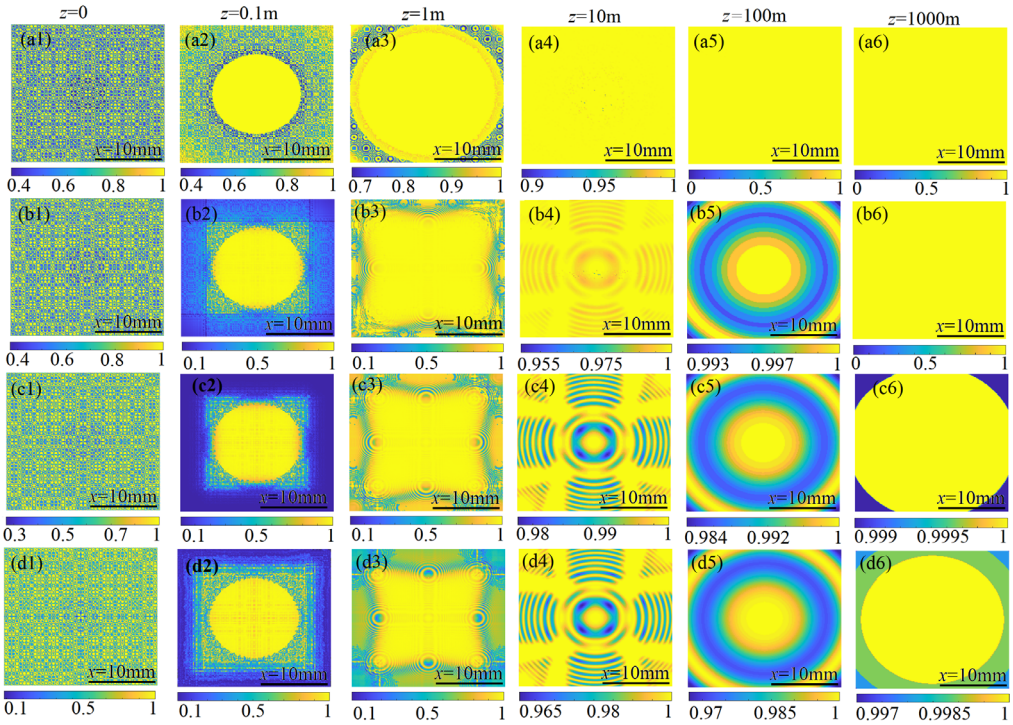

Fig. 5. The transverse $|\eta(\rho, -\rho)|$ distribution of an HNUC beam with different obstacles at different propagation distance distances. As a comparison, the first row shows the results without the obstacle. (a1)–(a6) $\omega_d = 0$ μm, (b1)–(b6) $\omega_d = 10$ μm, (c1)–(c6) $\omega_d = 25$ μm, and (d1)–(d6) $\omega_d = 50$ μm.

Figure 5 shows that the beam's transverse $|\eta(\rho, -\rho)|$ distribution varies with different obstacles at different propagation distances. For easier comparison, the first row presents the beam's transverse $|\eta(\rho, -\rho)|$ distribution without obstacle. The first column shows that on the source plane, the beam's coherence displays a non-uniform distribution. As the propagation distance increases, the beam coherence gradually approaches a uniform distribution, achieving coherence of 1 radially outward from the center. This result indicates that non-uniform, partially coherent light evolves into fully coherent light. Notably, when the propagation distance exceeds 10 m, the non-uniform, partially coherent light, even without obstacles, transforms fully coherent (as illustrated in Fig. 5(a5) and (a6)). Comparing the coherence distribution in the first row, it becomes evident that the obstacle sizes significantly affect the beam's coherence distribution. More considerable obstacles weaken the self-reconstructing ability of the beam's coherence, requiring a longer propagation distance to restore a uniform distribution, as shown in Fig. 5(a1)–(a6).

Figure 6 illustrates the influence of the transverse $|\eta(\rho, -\rho)|$ of the HNUC beam at various propagation distances when obstacles are located at different positions of the transverse section. The results indicate that the presence of obstacles alters the coherence distribution of the beam due to scattering and diffraction effects compared to

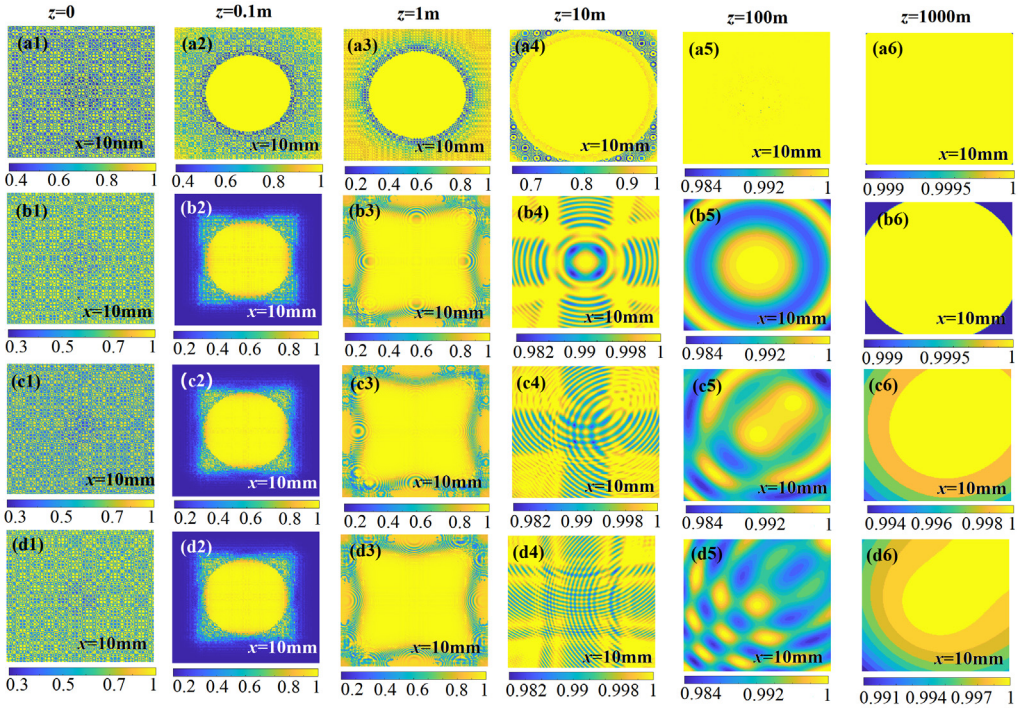

Fig. 6. The transverse $|\eta(\rho, -\rho)|$ distribution of an HNUC beam with different transverse position coordinates of the obstacle at different propagating distances. As a comparison, the first row shows the results without the obstacle. (a1)–(a6) $x_0 = y_0 = 0$, $\omega_d = 0$, (b1)–(b6) $x_0 = y_0 = 0$, $\omega_d = 25$ μm, (c1)–(c6) $x_0 = y_0 = 0.25$ mm, $\omega_d = 25$μm, and (d1)–(d6) $x_0 = y_0 = 0.5$mm, $\omega_d = 25$μm.

a situation without obstacles. Furthermore, the position of these obstacles can impact the symmetry of the coherence distribution, which interferes with the self-reconstructive process of the beam. Experimental results show a negative correlation between obstacle size and beam self-healing ability, meaning that the larger the obstacle, the weaker the self-reconstructive ability. However, as the propagation distance increases, the DOC of the beam gradually improves. Ultimately, the DOC of the beam approaches a fully coherent state, resembling the condition observed without obstacles.

Figure 7 illustrates how various beam source parameters influence the transverse $|\eta(\rho, -\rho)|$ of the HNUC beam at different propagation distances in the presence of obstacles. For comparison, the red curves represent the results obtained without any obstacles. As shown in Fig. 7, when the propagation distance is short, the positions of the obstacles and the beam source parameters, such as beam width, coherence length, and beam order, significantly affect the beam's coherence distribution. On the source plane, this coherence distribution changes dramatically and markedly differs from that of the HNUC beam when the propagation distance is less than 10 meters. Furthermore, as the propagation distance increases, this difference gradually diminishes. When the propagation distance exceeds 100 meters, the coherence distribution closely resembles that

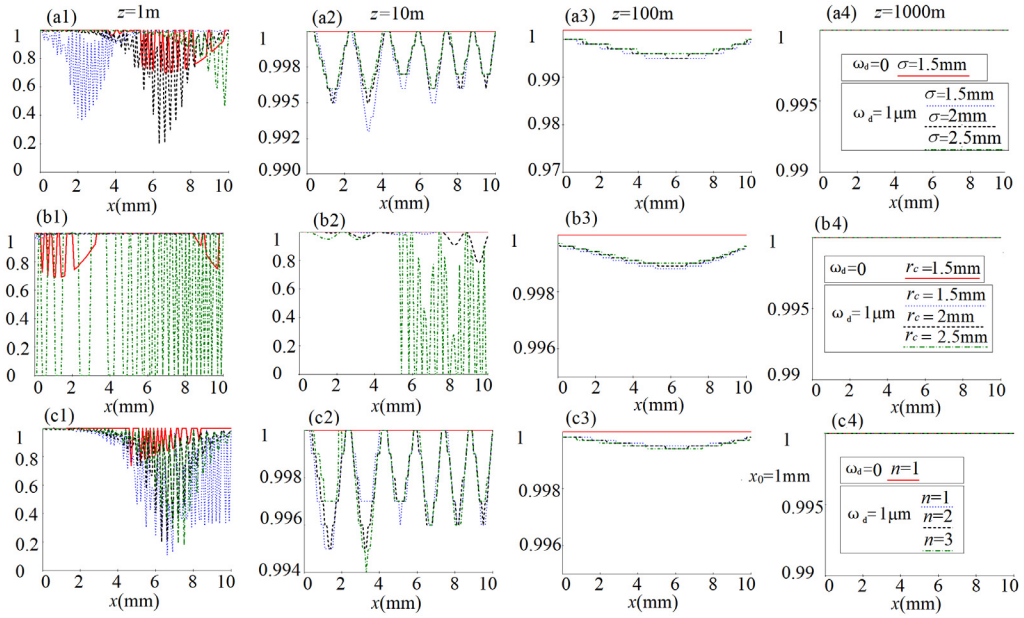

Fig. 7. The transverse $|\eta(\rho, -\rho)|$ distribution of an HNUC beam with different beam source parameters at different distances when encountering an obstacle. As a comparison, the red curves show the results without the obstacle (a1)–(a4) σ = 1.5, 2, 2.5 mm, and ω_d = 1 μm, (b1)–(b4) r_c = 1.5, 2, 2.5 mm, and ω_d = 1 μm, and (c1)–(c4) n = 1, 2, 3, and ω_d = 1 μm.

of an unobstructed light beam. The initially non-uniform coherent beam evolves into a fully coherent beam, and by the time the propagation distance surpasses 1 kilometer, the effects of obstacles and source parameters on the beam become negligible, leading to a coherence distribution consistent with that of an unobstructed light beam. These findings suggest that the beam's coherence demonstrates a self-reconstructing capability.

4. Conclusion

This study focused on Hermitian non-uniform correlation beams as a typical example of investigating the self-healing properties of vector beams with non-uniform correlation structures. Even when the beam encounters obstacles, its intensity distribution still shows a notable self-focusing phenomenon. The intrinsic characteristics of non-uniform light beams help offset the effects of obstacle scattering, allowing the beam to self-reconstruct within the focal length range. Beyond this range, the self-reconstructive ability of the beam depends on the size of the obstacles and the source parameters of the beam. Additionally, obstacles impact the coherence and polarization distribution of the beam; as the propagation distance increases, the DOC distributions of the beam return to their original states.

Disclosures
The authors declare no conflict of interest.

Data availability
Data underlying the results presented in this paper are not publicly available at this time but may be obtained from the authors upon reasonable request.

References

[1] Korotkova O., Andrews L.C., Phillips R.L., *Model for a partially coherent Gaussian beam in atmospheric turbulence with application in Lasercom*, Optical Engineering **43**(2), 2004: 330-341. https://doi.org/10.1117/1.1636185

[2] Berman G.P., Gorshkov V.N., Torous S.V., *Scintillation reduction for laser beams propagating through turbulent atmosphere*, Journal of Physics B **44**(5), 2011: 055402. https://doi.org/10.1088/0953-4075/44/5/055402

[3] Gbur G., *Partially coherent beam propagation in atmospheric turbulence*, Journal of the Optical Society of America A **31**(9), 2014: 2038-2045. https://doi.org/10.1364/JOSAA.31.002038

[4] Mao H., Chen Y., Liang C., Chen L., Cai Y., Ponomarenko S.A., *Self-steering partially coherent vector beams*, Optics Express **27**(10), 2019: 14353-14368. https://doi.org/10.1364/OE.27.014353

[5] Yu J., Chen Y., Liu L., Liu X., Cai Y., *Splitting and combining properties of an elegant Hermite -Gaussian correlated Schell-model beam in Kolmogorov and non-Kolmogorov turbulence*, Optics Express **23**(10), 2015: 13467-13481. https://doi.org/10.1364/OE.23.013467

[6] Mei Z., *Light sources generating self-focusing beams of variable focal length*, Optics Letters **39**(2), 2014: 347-350. https://doi.org/10.1364/OL.39.000347

[7] Gori F., Santarsiero M., *Devising genuine spatial correlation functions*, Optics Letters **32**(24), 2007: 3531-3533. https://doi.org/10.1364/OL.32.003531

[8] Gori F., Ramírez-Sánchez V., Santarsiero M., Shirai T., *On genuine cross-spectral density matrices*, Journal of Optics A: Pure and Applied Optics **11**(8), 2009: 085706. https://doi.org/10.1088/1464-4258/11/8/085706

[9] Yu J., Zhu X., Lin S., Wang F., Gbur G., Cai Y., *Vector partially coherent beams with prescribed non-uniform correlation structure*, Optics Letters **45**(13), 2020: 3824-3827. https://doi.org/10.1364/OL.397316

[10] Vyas S., Niwa M., Kozawa Y., Sato S., *Diffractive properties of obstructed vector Laguerre -Gaussian beam under tight focusing condition*, Journal of the Optical Society of America A **28**(7), 2011: 1387-1394. https://doi.org/10.1364/JOSAA.28.001387

[11] Wu D., Wang F., Cai Y., *High-order nonuniformly correlated beams*, Optics & Laser Technology **99**, 2018: 230-237. https://doi.org/10.1016/j.optlastec.2017.09.007

[12] Gu Y., Gbur G., *Scintillation of pseudo-Bessel correlated beams in atmospheric turbulence*, Journal of the Optical Society of America A **27**(12), 2010: 2621-2629. https://doi.org/10.1364/JOSAA.27.002621

[13] Song Z., Liu Z., Zhou K., Sun Q., Liu S., *Propagation characteristics of a non-uniformly Hermite -Gaussian correlated beam*, Journal of Optics **18**(1), 2015: 015606. https://doi.org/10.1088/2040-8978/18/1/015606

[14] Lin S., Wang C., Zhu X., Lin R., Wang F., Gbur G., Cai Y., Yu J., *Propagation of radially polarized Hermite non-uniformly correlated beams in a turbulent atmosphere*, Optics Express **28**(19), 2020: 27238-27249. https://doi.org/10.1364/OE.402021

[15] MacDonald R.P., Boothroyd S.A., Okamoto T., Chrostowski J., Syrett B.A., *Interboard optical data distribution by Bessel beam shadowing*, Optics Communications **122**(4-6), 1996: 169-177. https://doi.org/10.1016/0030-4018(95)00432-7

[16] OTTE E., NAPE I., ROSALES-GUZMÁN C., VALLÉS A., DENZ C., FORBES A., *Recovery of nonseparability in self-healing vector Bessel beams*, Physical Review A **98**, 2018: 053818. https://doi.org/10.1103/PhysRevA.98.053818
[17] SOGOMONIAN S., KLEWITZ S., HERMINGHAUS S., *Self-reconstruction of a Bessel beam in a nonlinear medium*, Optics Communications **139**(4-6), 1997: 313-319. https://doi.org/10.1016/S0030-4018(97)00093-X
[18] VYAS S., KOZAWA Y., SATO S., *Self-healing of tightly focused scalar and vector Bessel–Gauss beams at the focal plane*, Journal of the Optical Society of America A **28**(5), 2011: 837-843. https://doi.org/10.1364/JOSAA.28.000837
[19] WANG F., CHEN Y., LIU X., CAI Y., PONOMARENKO S.A., *Self-reconstruction of partially coherent light beams scattered by opaque obstacles*, Optics Express **24**(21), 2016: 23735-23746. https://doi.org/10.1364/OE.24.023735
[20] WU G., WANG F., CAI Y., *Generation and self-healing of a radially polarized Bessel-Gauss beam*, Physical Review A **89**(4), 2014: 043807. https://doi.org/10.1103/PhysRevA.89.043807
[21] LIU X., PENG X., LIU L., WU G., ZHAO C., WANG F., CAI Y., *Self-reconstruction of the degree of coherence of a partially coherent vortex beam obstructed by an opaque obstacle*, Applied Physics Letters **110**(18), 2017: 181104. https://doi.org/10.1063/1.4982786
[22] PENG X., WANG H., LIU L., WANG F., POPOV S., CAI Y., *Self-reconstruction of twisted Laguerre -Gaussian Schell-model beams partially blocked by an opaque obstacle*, Optics Express **28**(21), 2020: 31510-31523. https://doi.org/10.1364/OE.408357
[23] ZHOU Y., CUI Z., HAN Y., *Polarization and coherence properties in self-healing propagation of a partially coherent radially polarized twisted beam*, Optics Express **30**(13), 2022: 23448-23462. https://doi.org/10.1364/OE.462642
[24] MEYSTRE P., *Introduction to the theory of coherence and polarization of light*, Physics Today **61**(12), 2008: 59-60. https://doi.org/10.1063/1.3047693

Received April 20, 2025
in revised form May 15, 2025